Clinical Kidney Journal

Clinical Kidney Journal, 2024, vol. 17, no. 5, sfae064

https://doi.org/10.1093/ckj/sfae064
Advance Access Publication Date: 14 March 2024
Original Article

ORIGINAL ARTICLE

[^{18}F] AlF-NOTA-FAPI-04 PET/CT for non-invasive assessment of tubular injury in kidney diseases

Hao Wang[1,*], Ping Zhang[2,*], Wei Wang[2,*], Limeng He[1], Nan Liu[1], Juan Yang[2], Deying Tang[2], Guisen Li[2], Yunlin Feng[2] and Wei Zhang[1]

[1]Department of Nuclear Medicine, Sichuan Provincial People's Hospital, University of Electronic Science and Technology of China, Chengdu, Sichuan, China; and [2]Department of Nephrology, Sichuan Provincial People's Hospital, University of Electronic Science and Technology of China, Chengdu, Sichuan, China

*These authors contributed equally to this work and should be considered co-first authors.
Correspondence to: Wei Zhang; E-mail: zhangwscd@uestc.edu.cn; Yunlin Feng; E-mail: fengyunlin@med.uestc.edu.cn

ABSTRACT

Background. [^{18}F] AlF-NOTA-FAPI-04 is a novel positron emission tomography (PET) ligand, which specifically targets fibroblast activation protein (FAP) expression as a FAP inhibitor (FAPI). We analysed the diagnostic value of [^{18}F] AlF-NOTA-FAPI-04 PET/CT for the non-invasive assessment of kidney interstitial inflammation and fibrosis in different renal pathologies.

Methods. Twenty-six patients (14 males and 12 females; mean age, 50.5 ± 16.5 years) with a wide range of kidney diseases and 10 patients (six males and four females; mean age, 55.4 ± 8.6 years) without known evidence of renal disease as disease controls underwent [^{18}F] AlF-NOTA-FAPI-04 PET/CT imaging. Kidney tissues obtained from kidney biopsies were stained with haematoxylin and eosin, periodic acid-Schiff, Masson's trichome, and periodic acid–silver methenamine. Immunohistochemical staining was also performed to assess the expression of α-smooth muscle actin (αSMA) and FAP. Renal parenchymal FAPI uptake reflected by maximum standardized uptake value (SUV_{max}) and mean standardized uptake value (SUV_{mean}) measurements on PET/CT was analysed against pathohistological findings.

Results. We found that renal parenchymal FAPI uptake was significantly higher in patients with various kidney diseases than in control patients in this study (SUV_{max} = 4.3 ± 1.8 vs 1.9 ± 0.4, SUV_{mean}=3.9 ± 1.7 vs 1.5 ± 0.4, respectively; all $P < 0.001$). All kidney diseases, both in acute and chronic kidney disease, had increased renal parenchymal uptake to varying degrees. The correlation analysis indicated a positive association between the SUV_{max} and the tubulointerstitial inflammation (TII), interstitial fibrosis and tubular atrophy (IF/TA), and TII + IF/TA scores (r = 0.612, 0.681, and 0.754, all $P < 0.05$), and between the SUV_{mean} and the TII, IF/TA, and TII + IF/TA scores (r = 0.603, 0.700, and 0.748, all $P < 0.05$). Furthermore, we found significant positive correlations between both SUV_{max} and the SUV_{mean} with SMA and FAP staining scores (r = 0.686 and 0.732, r = 0.667 and 0.739, respectively; both $P < 0.001$).

Conclusions. [^{18}F] AlF-NOTA-FAPI-04 PET/CT is clinically available for the comprehensive and non-invasive assessment of tubular injury in various kidney diseases.

Received: 13.12.2023; Editorial decision: 16.2.2024

© The Author(s) 2024. Published by Oxford University Press on behalf of the ERA. This is an Open Access article distributed under the terms of the Creative Commons Attribution-NonCommercial License (https://creativecommons.org/licenses/by-nc/4.0/), which permits non-commercial re-use, distribution, and reproduction in any medium, provided the original work is properly cited. For commercial re-use, please contact journals.permissions@oup.com

GRAPHICAL ABSTRACT

Clinical Kidney Journal

[18F] AlF-NOTA-FAPI-04 PET/CT for non-invasive assessment of tubular injury in kidney diseases

To investigate the diagnostic value of [18F]AlF-NOTA-FAPI-04 PET/CT in patients with various kidney diseases, we analyzed the correlation between renal parenchymal uptake of FAPI and histological findings of kidney biopsies and renal function.

Methods

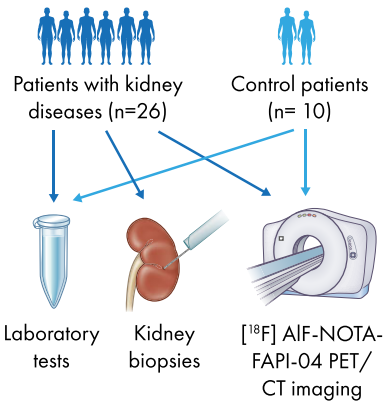

Results

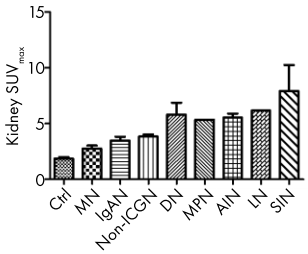

All kidney diseases had varying degrees of increased renal parenchymal uptake

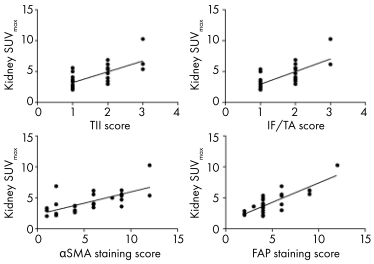

The uptake of FAPI increased proportionally with the severity of renal inflammation and interstitial fibrosis, exhibiting positive correlations with staining scores for aSMA and FAP

Conclusion: [18F] AlF-NOTA-FAPI-04 PET/CT is clinically available for the comprehensive and non-invasive assessment of tubular injury in various kidney diseases.

Wang H., Zhang P., Wang W., et al.
Clinical Kidney Journal (2024)
zhangwscd@uestc.edu.cn
fengyunlin@med.uestc.edu.cn
@CKJsocial

Keywords: [18F] AlF-NOTA-FAPI-04 PET/CT, fibroblast activation protein, fibrosis, inflammation, kidney disease

KEY LEARNING POINTS

What was known:

1. Early recognition and accurate evaluation of renal inflammation and fibrosis are critical in the management of kidney disease.
2. Currently, non-invasive functional parameters are unable to accurately and specifically reflect the intrarenal molecular processes.
3. [18F] AlF-NOTA-FAPI-04 is a novel positron emission tomography (PET) ligand that specifically targets fibroblast activation protein (FAP) expression as a FAP inhibitor (FAPI) and has been demonstrated to have high uptake in fibrotic diseases.

This study adds:

We provided the first evidence that:

1. The uptake of FAPI in renal parenchyma increased proportionally with the severity of renal inflammation and interstitial fibrosis, exhibiting positive correlations with staining scores for α-smooth muscle actin (αSMA) and FAP and negative correlation with the eGFR.
2. Increased renal parenchymal FAPI uptake was consistently observed among all kidney diseases in this study. Patients without known kidney diseases had mild uptake of FAPI in the renal parenchyma.

Potential impact:

1. Our findings suggested that [18F] AlF-NOTA-FAPI-04 PET/CT is clinically available for the comprehensive and non-invasive assessment of tubular injury in various kidney diseases.
2. We hope our results help to shed light on the value of this novel molecular imaging in assessment of inflammation and fibrosis in kidney diseases.

INTRODUCTION

Renal inflammation plays a pivotal role in initiating and accelerating renal dysfunction in various kidney diseases [1], as does renal interstitial fibrosis, which consistently represents an advanced stage of renal inflammation [2]. After prolonged inflammation, progressive fibrosis occurs due to excessive accumulation of fibroblast and myofibroblast, along with increased production of extracellular matrix [3]. Fibrosis is often seen in the tubulointerstitial area as the diagnosed kidney disease progresses. This process represents the common pathological pathway observed in almost all chronic nephropathies [4, 5]. Therefore, early recognition and accurate evaluation of renal inflammation and fibrosis are critical in the management of kidney disease. Although histopathological analysis of kidney biopsy samples can provide direct evidence of renal inflammation and fibrosis, it is limited by local sampling and carries a risk of bleeding [6]. Magnetic resonance imaging has been proven to be a useful non-invasive assessment tool for evaluating renal fibrosis [7], however, it still lacks sensitivity and quantification in evaluating renal inflammation [8].

Molecular imaging enables a non-invasive, comprehensive, and quantitative evaluation of physiological or pathological processes by integrating imaging technologies with specific molecular probes [6]. Currently, the major molecular imaging for visualizing inflammation is ^{18}F-fluoro-2-deoxyglucose (^{18}F-FDG) positron emission tomography/computed tomography (PET/CT), in which the ^{18}F-FDG accumulates in areas with acute inflammation [9].

FAP is a cell surface dipeptidyl peptidase family member of serine proteases [10]. Abnormal expression of FAP can be observed not only in neoplastic diseases, but also in inflammatory and benign fibrotic tissues including the liver and lung [11–13]. Recent studies have demonstrated increased uptake of FAPI-based radiopharmaceuticals in inflammatory and fibrotic regions in cancer [9]. The ^{68}Ga-FAPI binds to FAP in fibroblasts of tumour tissue [14, 15]. A preclinical study has shown that ^{68}Ga-FAPI-04 PET/CT can identify renal fibrosis quickly and non-invasively compared to renal biopsy [16]. A recent clinical study demonstrated that the accumulation of ^{68}Ga-FAPI on PET/CT correlated to the severity of kidney fibrosis defined by immunohistopathology [17]. Another clinical study with a larger sample showed that the FAPI uptake increased when glomerular filtration rate decreased [18]. All three studies highlighted the value of ^{68}Ga-FAPI for non-invasive and quantitative assessment of kidney fibrosis and renal dysfunction. However, although ^{68}Ga labelled FAPI is currently standard for FAPI-PET, its batch activity is limited [19]. The short half-life of ^{68}Ga (68 min) can cause problems in production and delivery. [^{18}F] AlF-NOTA-FAPI-04 presents a potentially promising alternative that combines the advantages of a chelator-based radiolabelling method with the unique properties offered by fluorine-18, allowing more practical large-scale production [20]. ^{18}F is advantageous for future mass production due to its higher positron yield and superior electron energy. Furthermore, it has been shown that the maximum positron energy and thus the mean range in tissue is different between ^{68}Ga and ^{18}F: positrons produced by the decay of ^{68}Ga have an end-point energy three times higher than that of ^{18}F and therefore have a much larger mean range in tissue (^{68}Ga 3.5 mm; ^{18}F 0.6 mm). This reduces the spatial resolution of ^{68}Ga PET [21].

Therefore, we investigated the efficacy of [^{18}F] AlF-NOTA-FAPI-04 PET/CT imaging in evaluating renal inflammation and fibrosis in different kidney diseases and the correlation between renal parenchymal uptake of ^{18}F-FAPI with histological findings from kidney biopsies and renal function.

MATERIALS AND METHODS

Study design and population

This was a prospective study. All kidney disease patients scheduled for kidney biopsy at Sichuan Provincial People's Hospital between September 2022 and May 2023 were invited to participate this study. Controls consisted of patients who underwent PET/CT examination for non-kidney diseases during the same period, had normal serum creatinine, and tested negative for proteinuria. Written informed consent was obtained from all patients. This study was approved by the institutional review board of Sichuan Provincial People's Hospital (no. 2022–203) and registered on the Clinical Trial Register (Identifier no. NCT05752097). All procedures were in accordance with the ethical standards of the institutional and national research committees and with the 1964 Helsinki declaration and its later amendments or comparable ethical standards. Exclusion criteria were patients with severe bleeding disorders preventing renal puncture biopsy; comorbid chronic liver disease, myocardial infarction, stroke, malignancy; inability to cooperate with renal puncture biopsy due to verbal communication or other problems; and pregnant (or planning to become pregnant within 6 months) or lactating. Patients were also excluded if they had uncontrolled cardiopulmonary disease or a mental abnormality that made them unable to tolerate PET/CT examination.

The study collected basic demographic information, including gender and age. Before the PET/CT examinations, serum creatinine (Cr) results were extracted from the hospital's electronic informative system for the calculation of estimated glomerular filtration rate (eGFR) using the Chronic Kidney Disease Epidemiology Collaboration (CKD-EPI) equation [22].

Synthesis of radiopharmaceuticals

The automatic synthesis procedure of [^{18}F] AlF-NOTA-FAPI-04 was carried out as described previously [20]. The final product [^{18}F] AlF-NOTA-FAPI-04 underwent quality control analysis using instant thin-layer chromatography assessment. The radiochemical purity of the final product exceeded 95%.

PET/CT imaging acquisition

All patients underwent [^{18}F] AlF-NOTA-FAPI-04 PET/CT examinations. Before the examinations, all patients were instructed to urinate to minimize potential image quality interference caused by residual radioactive tracers in the renal pelvis and calyx. The PET/CT imaging was conducted 52.4 ± 10.5 minutes after administering an injection of [^{18}F] AlF-NOTA-FAPI-04 at a dosage of 3.70–4.44 MBq (0.10–0.12 mCi)/kg (using FlowMotion scanning technology). A low-dose CT (120 keV; 50 mAs; 1.3 pitch; 3 mm slice thickness; 0.5 seconds rotation time; estimated radiation dose, 9.0 mGy) was initially performed for attenuation correction and anatomical localization from the tip of the skull to the mid-thigh, followed by a subsequent PET scan lasting for a duration of 12 min using a PET/CT scanner (Biograph mCT Flow 64, Siemens, Germany). The acquired data were reconstructed using the ordered subset expectation maximization method (two iterations, 21 subsets).

Imaging analysis

The PET/CT images were independently assessed by two nuclear medicine physicians with more than 5 years of experience

in interpreting PET/CT images, in a random order. Readers were blinded to clinical data and performed a consensus image interpretation. Both visual and quantificational analyses were employed. For the visual analysis, a three-scale grading system was used: mild uptake for uptake comparable to or slightly higher than that of the blood pool, moderate uptake for uptake equivalent to two to three times that of the blood pool, and intense uptake for significantly greater uptake than that of the blood pool. For quantificational analysis, the maximum standardized uptake value (SUV_{max}) and the mean standardized uptake value (SUV_{mean}) normalized to body weight were calculated. Renal tracer uptake was quantified using SUV_{max} or SUV_{mean} at distinct locations within the renal parenchyma (superior, middle, and inferior renal cortex), as previously described [18]. The mean SUV_{max} or SUV_{mean} at these three different locations in the renal parenchymal were then calculated as the renal parenchyma SUV_{max} or SUV_{mean}.

Pathohistological examinations

Patients with kidney disease underwent a kidney biopsy on the second day after the PET/CT scan. The kidney tissues obtained from biopsies were fixed in formalin and embedded in paraffin before being sectioned into 2-μm-thick slices. These sections underwent staining with haematoxylin and eosin, periodic acid-Schiff, Masson trichome, and periodic acid–silver methenamine. Additionally, immunohistochemical staining was performed to assess the expressions of α-smooth muscle actin (αSMA) and FAP using SMA-alpha antibody (diluted at 1:200, M50132; Zhengneng, Chengdu, China) and FAP-alpha antibody (diluted at 1:1000, ab53066; Abcam, Cambridge, MA, USA), respectively.

In view of the mild degree of inflammation and fibrosis in the nephritis and nephropathy patients enrolled in this study, we used a modified scoring scale compared to previous study [23]. The severity of interstitial fibrosis and tubular atrophy (IF/TA) was assessed based on the presence and extent of IF/TA lesions observed in kidney tissues stained with Masson trichrome, using a scale ranging from 1 to 3 ($1 \leq 5\%$; 2 = 5–25%; $3 \geq 25\%$). Tubulointerstitial inflammation (TII) was evaluated by scoring the degree of interstitial inflammatory infiltrate observed in tissue sections, using a scale ranging from 1 to 3 ($1 \leq 5\%$, 2 = 5–25%, $3 \geq 25\%$). αSMA or FAP-positive cells were identified as cells exhibiting brown-yellow granules or masses on corresponding staining under light microscopy at a resolution of ×200. Both the intensity and percentage of positive staining were evaluated. Staining intensity was graded on a scale from 0 to 3 (0 = undetectable; 1 = faint buff; 2 = moderate buff; 3 = high buff or sepia). The extent of positive staining was scored based on the percentage of positive cells in all cells relative to all cells within the field of view, using a scale from 0 to 4 (0 = absence, $1 \leq 25\%$, 2 = 25 to < 50%, 3 = 50 to $\leq 75\%$, $4 \geq 75\%$). An integrated score for αSMA or FAP was calculated by multiplying the staining intensity with the percentage of positive cells.

The histopathological sections were examined by two experienced nephropathologists who were blinded to clinical data and PET/CT imaging results. All results were obtained by averaging the values from 10 fields of view. Any discrepancies were resolved through consensus.

Statistical analysis

Statistical analyses were conducted using SPSS 22.0 (SPSS Inc., Chicago, IL, USA). A normality test was performed on the quantitative variable. Continuous variables were presented as mean ± standard deviation (SD) or median and appropriate range. Inter-group comparisons were carried out using the Student's *t*-test. Categorical variables were described as rates or percentages and compared using the Chi-square test. Correlation analyses were conducted using Pearson correlation coefficients or Spearman rank correlation coefficients. A two-sided *P* value <0.05 was considered statistically significant.

RESULTS

Characteristics of the study population

A total of 26 patients with a various of kidney diseases (14 males and 12 females; mean age, 50.5 ± 16.5 years) were enrolled in Group A. The renal pathological diagnoses included IgA nephropathy ($n = 8$), membranous nephropathy ($n = 6$), acute interstitial nephritis ($n = 3$), non-immune complex glomerulopathy ($n = 3$), subacute interstitial nephritis ($n = 2$), diabetic nephropathy ($n = 2$), mesangial proliferative nephropathy ($n = 1$), and lupus nephritis ($n = 1$). Additionally, a control group (Group B) consisting of 10 patients without any evidence of kidney disease was enrolled (six males and four females; mean age, 55.4 ± 8.6 years). There were no statistically significant differences observed in terms of age or sex between the two groups. The eGFR in Group A was found to be significantly lower than that in Group B (65.2 ± 31.9 vs 100.0 ± 15.5, respectively; $P < 0.001$). The value of serum creatinine in Group A was significantly higher than that in Group B (135.1 ± 82.6 vs 66.9 ± 16.0, respectively; $P < 0.001$). The detailed characteristics of the study population are presented in Table 1.

Renal parenchymal FAPI uptake in the study population

The SUV_{max} and SUV_{mean} in Group A were found to be significantly higher than that in Group B (4.3 ± 1.8 vs 1.9 ± 0.4 and 3.9 ± 1.7 vs 1.5 ± 0.4, respectively; $t = 6.275$ and 6.479, all $P < 0.001$) (Table S1). Visual examination of FAPI imaging revealed varying degrees of renal parenchymal uptake in all 26 patients with kidney diseases, with patients 7, 11, and 8 exhibiting mild, moderate, and intense uptake, respectively (Table S2). Acute interstitial nephritis, subacute interstitial nephritis, mesangial proliferative nephropathy, and lupus nephritis exhibited the highest proportion of intense renal FAPI uptake (Figs 1 and 2). Patients with non-immune complex glomerulopathy and diabetic nephropathy demonstrated moderate to intense renal FAPI uptake (Fig. 3). Patients with IgA nephropathy or membranous nephropathy displayed mild to moderate renal FAPI uptake (Fig. 4). It is noteworthy that intense FAPI uptake in the renal parenchyma were observed in both acute and chronic kidney diseases (Figs S1 and S2). All 10 patients in the control group exhibited mild renal parenchymal uptake on visual interpretation.

Association between renal parenchymal FAPI uptake and severities of renal interstitial inflammation and fibrosis

The SUV_{max} in patients with mild renal interstitial inflammation (TII score = 1) was significantly lower compared to those with moderate or severe renal interstitial inflammation (TII score ≥ 2) (3.4 ± 1.1 vs 5.2 ± 1.9, respectively; $t = -3.000$, $P = 0.006$) (Fig. 5A). Similarly, the SUV_{mean} in patients with mild renal interstitial inflammation (TII score = 1) was significantly lower compared to those with moderate or severe renal interstitial inflammation

Table 1: Characteristics of the study population ($n = 36$).

Groups	Male, *n* (%)	Age (years) Mean ± SD	eGFR (ml/min/1.73 m^2) Mean ± SD	Serum Cr (μmol/l) Mean ± SD
Group A ($n = 26$)	14 (53.8)	50.5 ± 16.5	65.2 ± 31.9	135.1 ± 82.6
Group B ($n = 10$)	6 (60)	55.4 ± 8.6	100.0 ± 15.5	66.9 ± 16.0
P value	0.739	0.261	0.001	<0.001

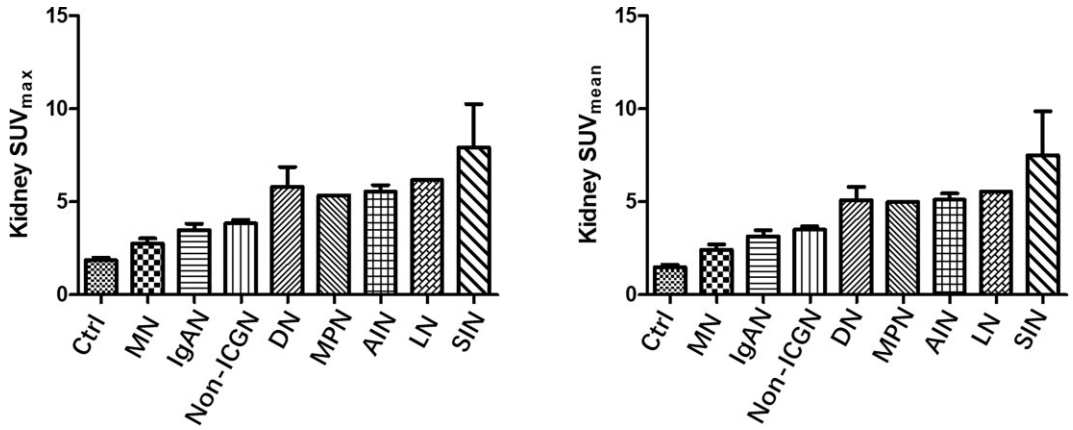

Figure 1: The FAPI uptake in the renal parenchyma varies among different kidney diseases. Distribution of kidney SUV_{max} and SUV_{mean} were observed to differ across these renal diseases. Ctrl indicates patients in the control group. Abbreviations: AIN: acute interstitial nephritis; DN: diabetic nephropathy; IgAN: IgA nephropathy; LN: lupus nephritis; MN: membranous nephropathy; MPN: mesangial proliferative nephropathy; non-ICGN: non-immune complex glomerulopathy; SIN: subacute interstitial nephritis.

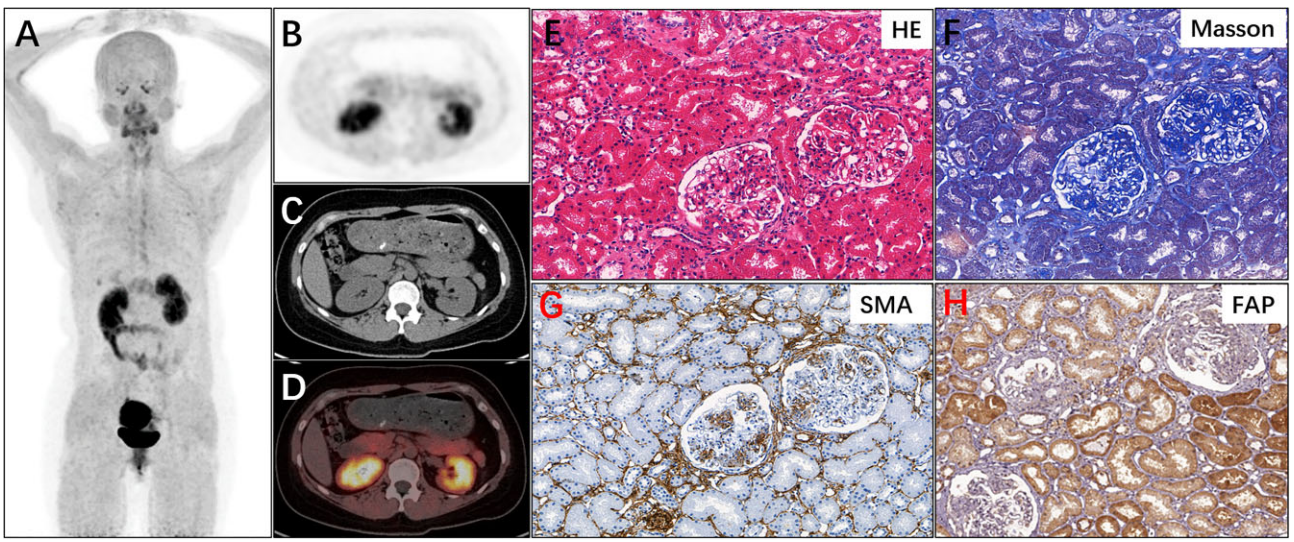

Figure 2: The renal parenchymal FAPI uptake and histological observations in a patient with lupus nephritis. A 28-year-old woman presented with albuminuria for 2 months. (**A**) The maximum intensity projection (MIP) image obtained from whole-body [^{18}F] AlF-NOTA-FAPI-04 PET/CT revealed diffuse uptake of radiotracer in both kidneys. (**B–D**) The cross-sectional images demonstrated intense radiotracer uptake within renal parenchyma, with SUV_{max} and SUV_{mean} values of 6.17 and 5.54, respectively. The pathological examination led to a diagnosis of diffuse proliferative lupus nephritis (TII score = 2, IF/TA score = 3) (**E** and **F**). Immunohistochemical analysis revealed prominent expression of αSMA and abundant FAP in the renal interstitium and tubules (αSMA staining score = 6, FAP staining score = 9) (**G** and **H**).

(TII score $\geq$ 2) (3.0 ± 1.1 vs 4.8 ± 1.9, respectively; $t = -2.883$, $P = 0.008$) (Fig. 5B). Among the 13 patients with mild interstitial inflammation, there were six, six, and one patients exhibiting mild, moderate, and intense renal parenchymal uptake, respectively. Among another group of 13 patients who had moderate or severe interstitial inflammation, there were one, five, and seven patients exhibiting mild, moderate, and intense renal parenchymal uptake, respectively (Table S3).

The assessment of interstitial fibrosis exhibited similar trends. The SUV_{max} and SUV_{mean} were significantly lower in

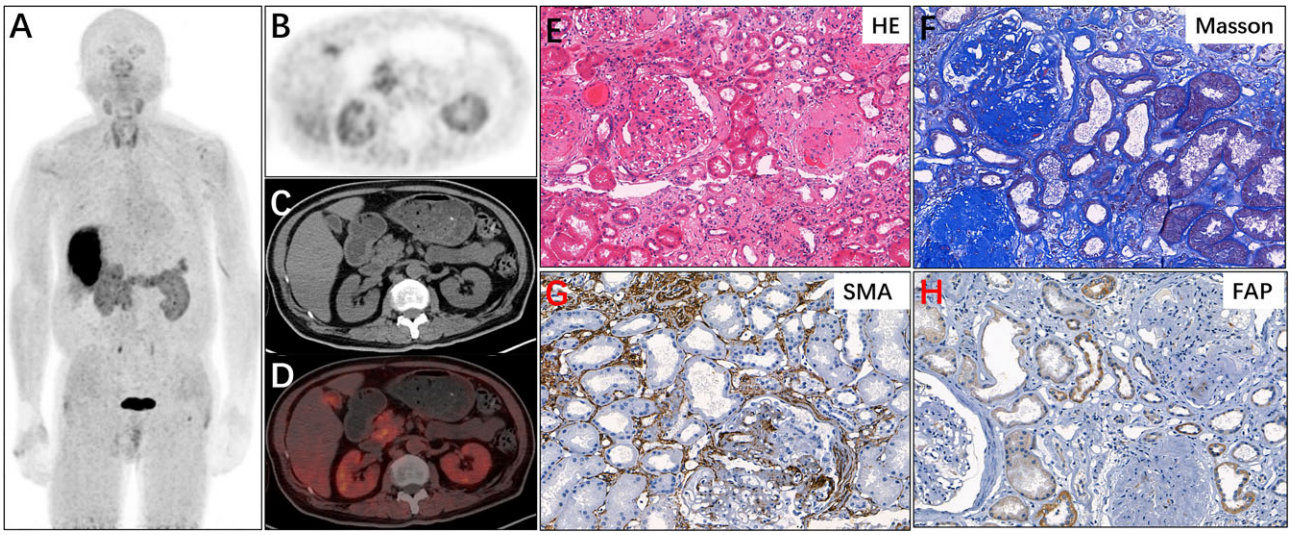

Figure 3: The renal parenchymal FAPI uptake and histological observations in a patient with diabetic nephropathy. A 60-year-old man with a history of diabetes presented with bilateral lower limb oedema and albuminuria for 2 months. (**A**) The MIP image obtained from whole-body [^{18}F] AlF-NOTA-FAPI-04 PET/CT revealed diffuse radiotracer uptake in both kidneys. (**B–D**) The cross-sectional images demonstrated moderate radiotracer uptake in the renal parenchyma, with SUV_{max} and SUV_{mean} values of 4.72 and 4.38, respectively. Subsequent renal pathological examination confirmed the diagnosis of diabetic nephropathy (TII score = 2, IF/TA score = 2) (**E** and **F**). Immunochemical analysis revealed moderate expression of αSMA and mild expression of FAP in the renal interstitium and tubules (αSMA staining score = 9, FAP staining score = 4) (**G** and **H**).

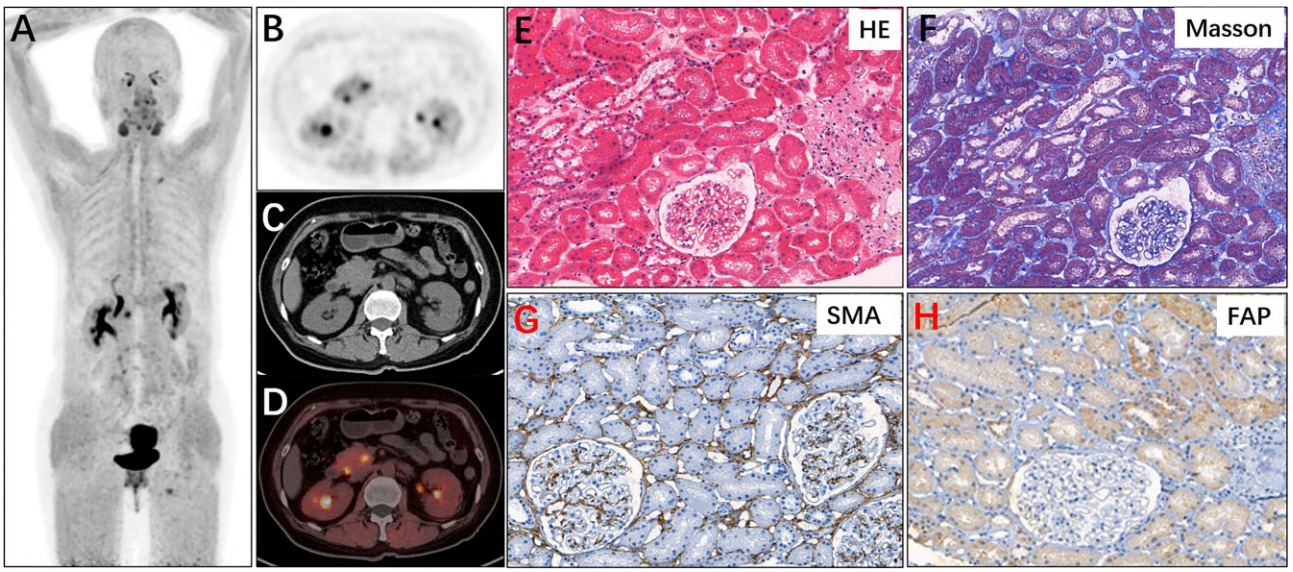

Figure 4: The renal parenchymal FAPI uptake and histological observations in a patient with membranous nephropathy. A 26-year-old male presented with lower limb oedema and albuminuria for 1 month. (**A**) The MIP image of whole-body [^{18}F] AlF-NOTA-FAPI-04 PET/CT scan revealed heterogeneous uptake of radiotracer in both kidneys. (**B–D**) The cross-sectional images showed mild radiotracer uptake in the renal parenchyma, with SUV_{max} and SUV_{mean} values of 2.23 and 1.95, respectively. Renal pathological examination confirmed a diagnosis of stage I–II membranous nephropathy (TII score = 1, IF/TA score = 1) (**E** and **F**). Immunochemical analysis revealed mild expression of αSMA and FAP in the renal interstitium and tubules (αSMA staining score = 4, FAP staining score = 2) (**G** and **H**).

patients with mild interstitial fibrosis and tubular atrophy (IF/TA score = 1) compared to those with moderate or higher levels of interstitial fibrosis and tubular atrophy (IF/TA score $\geq$ 2) (3.2 $\pm$ 1.1 vs 5.1 $\pm$ 1.8 and 2.8 $\pm$ 1.0 vs 4.7 $\pm$ 1.7, respectively; $t = -3.080$ and -3.079, all $P = 0.005$) (Fig. 5C and D). The proportion of mild uptake in patients with IF/TA score = 1 (6/11) was higher than that in patients with IF/TA score $\geq$ 2 (1/15) (Table S4).

The correlation analysis indicated positive association between the SUV_{max} of the renal parenchyma and the TII, IF/TA, and TII + IF/TA scores (r = 0.612, 0.681, and 0.754, all $P < 0.05$) (Fig. 6A–C and Table S5), and between the SUV_{mean} of the renal parenchyma and the TII, IF/TA, and TII + IF/TA scores (r = 0.603, 0.700, and 0.748, all $P < 0.05$) (Fig. 6D–F and Table S5).

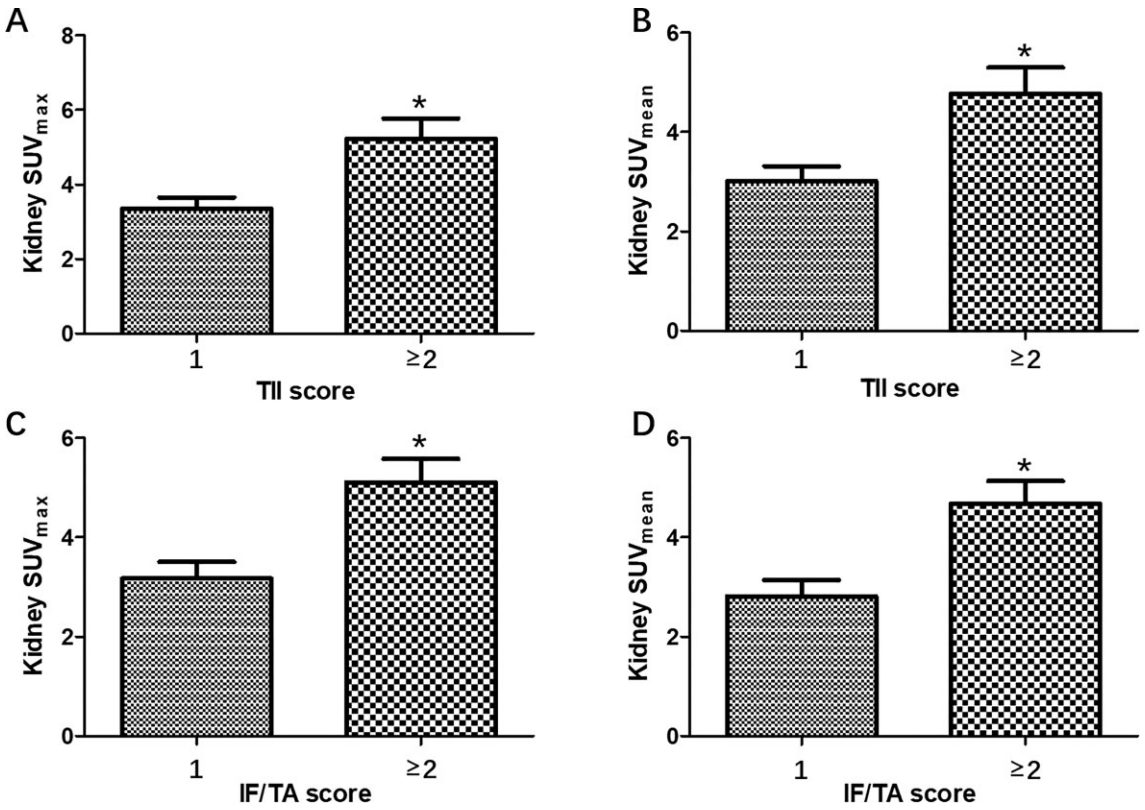

Figure 5: Comparison of the renal parenchymal FAPI uptake between patients with different severities of interstitial inflammation and fibrosis. (**A**) The SUV_{max} in patients with mild renal interstitial inflammation (TII score = 1) was significantly lower compared to those with moderate or higher levels of renal interstitial inflammation (TII score ≥ 2) (3.4 ± 1.1 vs 5.2 ± 1.9, respectively; $t = -3.000$, $P = 0.006$). (**B**) The SUV_{mean} in patients with mild renal interstitial inflammation (TII score = 1) was significantly lower compared to those with moderate or higher levels of renal interstitial inflammation (TII score ≥ 2) (3.0 ± 1.1 vs 4.8 ± 1.9, respectively; $t = -2.883$, $P = 0.008$). (**C**) The SUV_{max} in patients with mild interstitial fibrosis and tubular atrophy (IF/TA score = 1) was significantly lower compared to those with moderate or higher levels of interstitial fibrosis and tubular atrophy (IF/TA score ≥ 2) (3.2 ± 1.1 vs 5.1 ± 1.8, respectively; $t = -3.080$, $P = 0.005$). (**D**) The SUV_{mean} in patients with mild interstitial fibrosis and tubular atrophy (IF/TA score = 1) was significantly lower compared to those with moderate or higher levels of interstitial fibrosis and tubular atrophy (IF/TA score ≥ 2) (2.8 ± 1.0 vs 4.7 ± 1.7, respectively; $t = -3.079$, $P = 0.005$).

Association between the renal parenchymal FAPI uptake and immunohistochemical staining of FAP and αSMA

The results of correlation analysis demonstrated significant positive correlation between the SUV_{max} of the renal parenchyma and the staining scores for αSMA and FAP ($r = 0.686$ and 0.732, both $P < 0.001$) (Fig. 7A and B and Table S6), and between the SUV_{mean} of the renal parenchyma and the staining scores for αSMA and FAP ($r = 0.667$ and 0.739, both $P < 0.001$) (Fig. 7C and D and Table S6). Similarly, there was a positive correlation observed between the interstitial IF/TA score and the staining scores for αSMA ($r = 0.438$, $P < 0.05$) (Fig. 7E and Table S7). A positive correlation was observed between the staining scores for FAP and the interstitial IF/TA score and the staining scores for αSMA ($r = 0.590$ and 0.420, both $P < 0.05$) (Fig. 7F and G and Table S8).

Association between the renal parenchymal FAPI uptake and renal function

The SUV_{max} and SUV_{mean} of renal parenchyma exhibited significant negative correlation with eGFR levels ($r = -0.683$ and -0.614, all $P < 0.001$) (Fig. 7H and I).

DISCUSSION

In this study, [^{18}F] AlF-NOTA-FAPI-04 PET/CT was used to investigate patients with various kidney diseases and exhibited promising potential in evaluating tubular injury. The uptake of FAPI in renal parenchyma increased proportionally with the severity of renal inflammation and interstitial fibrosis, exhibiting positive correlations with staining scores for αSMA and FAP and negative correlation with the eGFR. Furthermore, increased renal parenchymal FAPI uptake was consistently observed among all kidney diseases in this study. Patients without known kidney diseases had mild uptake of FAPI in the renal parenchyma.

Differential diagnosis and assessment of activity in kidney diseases heavily rely on the analyses of eGFR, urinary examinations, and tissue samples obtained through invasive kidney biopsies. Currently non-invasive functional parameters are unable to accurately and specifically reflect the intrarenal molecular processes during the evolution of kidney diseases [6]. Although kidney biopsy is considered the gold standard, it is constrained by random and localized sampling. The diagnosis may yield false negatives if focally distributed lesions are missed during biopsy. Additionally, careful consideration must be given to perioperative risks such as bleeding and thromboembolism in high-risk patients. Therefore, there is an

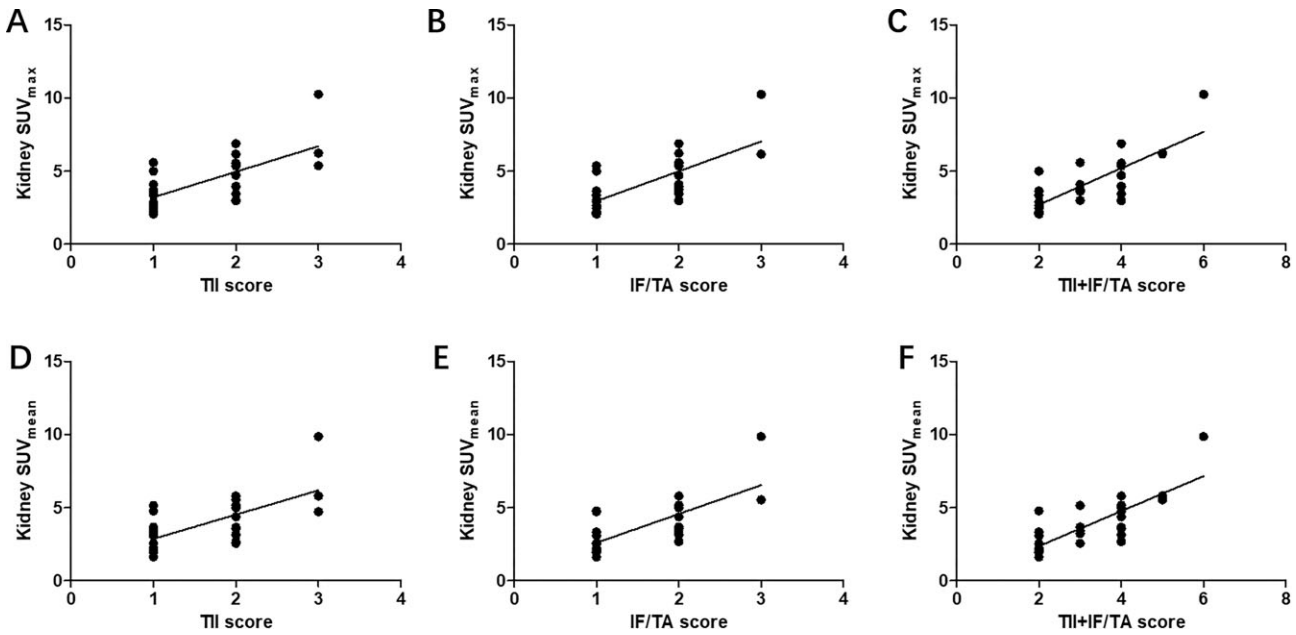

Figure 6: Correlation of the renal parenchymal FAPI uptake with the renal inflammation and fibrosis scores. (**A**) The SUV_{max} exhibited a positive correlation with the TII score ($r = 0.612$, $P = 0.001$). (**B**) The SUV_{max} demonstrated a positive correlation with the IF/TA score ($r = 0.681$, $P < 0.001$). (**C**) The SUV_{max} showed a positive correlation with the combined TII + IF/TA score ($r = 0.754$, $P < 0.001$). (**D**) The SUV_{mean} exhibited a positive correlation with the TII score ($r = 0.603$, $P = 0.001$). (**E**) The SUV_{mean} demonstrated a positive correlation with the IF/TA score ($r = 0.700$, $P < 0.001$). (**F**) The SUV_{mean} showed a positive correlation with the combined TII + IF/TA score ($r = 0.748$, $P < 0.001$).

urgent need for comprehensive and non-invasive assessment methods for kidney diseases. Molecular imaging might be a potential option to fill this gap.

[^{18}F] AlF-NOTA-FAPI-04 is a promising alternative to ^{68}Ga-FAPI-04, exhibiting high radiolabel yields and specific activities [24]. The higher yield of ^{18}F means that more production can be synthesized in a single labelling, allowing more patients to be examined, thereby reducing the cost per patient. In addition, the longer half-life of ^{18}F also allows delayed imaging in patients with renal disease, which facilitates better clearance of residual urine from the renal pelvis and calyces and allows more accurate measurement of renal cortical FAPI uptake. This study represents the first investigation into renal FAPI uptake patterns in kidney disease patients undergoing PET imaging using [^{18}F] AlF-NOTA-FAPI-04. The obtained PET/CT images demonstrate excellent contrast for detecting inflammation and fibrosis within the kidney. In comparison to localized sampling through renal biopsy, PET/CT examination enables comprehensive visualization of the entire kidney in a single scan.

Renal inflammation is the initial response to kidney stress or injury, serving as a protective mechanism against further damage [25]. Left unresolved, the inflammation can lead to progressive renal fibrosis and destruction of kidney structure and function, ultimately resulting in CKD [26, 27]. This highlights the crucial role that both inflammation and fibrosis play throughout the progression of kidney diseases. In fact, myofibroblasts accumulation is the predominant source of collagen production and a key event in renal fibrosis progression [5]. In this study, the FAP and αSMA staining was employed to reflect the extent of inflammation and fibrosis, respectively. We discovered a closely positive correlation between the intensity of renal parenchymal uptake on FAPI imaging and the staining scores for αSMA and FAP across all underlying kidney diseases based on visual interpretation. These findings confirmed from a histological perspective that visualization of FAP expression by [^{18}F] AlF-NOTA-FAPI-04 PET/CT imaging could aid the determination of the inflammation and interstitial fibrosis.

Furthermore, we found that FAP was predominantly expressed in the renal tubular epithelial cells (TECs), while αSMA was primarily expressed in the renal interstitium. These findings contradict existing literature where relatively mild FAP expression is mainly observed in glomeruli or interstitium, which does not align with high FAPI uptake seen in some PET/CT images [17]. This discrepancy may be attributed to several potential reasons for our results. To the best of our knowledge, the renal tubules and interstitium constitute a significant proportion of the kidney and serve as major sites for responding to injuries. Increasing evidence shows that renal TECs play diverse roles in either promoting renal repair or contributing to the progression of CKD [28]. Due to their innate immune characteristics, TECs can act as immune responders against various insults, leading to the production and release of bioactive mediators that drive interstitial inflammation and fibrosis [4, 29]. Immunohistochemical staining in our study confirmed both early tubular damage and advanced interstitial fibrosis in patients with different stages of kidney disease. As most of the patients we enrolled with kidney disease were in the early stages of kidney disease, we observed high levels of FAP expression in the renal TECs of many of them. These results indicate that [^{18}F] AlF-NOTA-FAPI-04 PET/CT imaging in patients with renal disease may reflect tubular injury at an earlier stage, in addition to the severity of renal inflammation and fibrosis.

Our finding that the renal parenchymal FAPI uptake is inversely correlated with eGFR level aligns with a previously published study [18]. However, we also found individual patients with low eGFR values and mild parenchymal FAP expression. The reason for this analysis may be that these patients were in the acute stage of kidney disease and, although they had poor renal function, they had not yet developed significant renal inflammation and fibrosis. Our study benefited from a

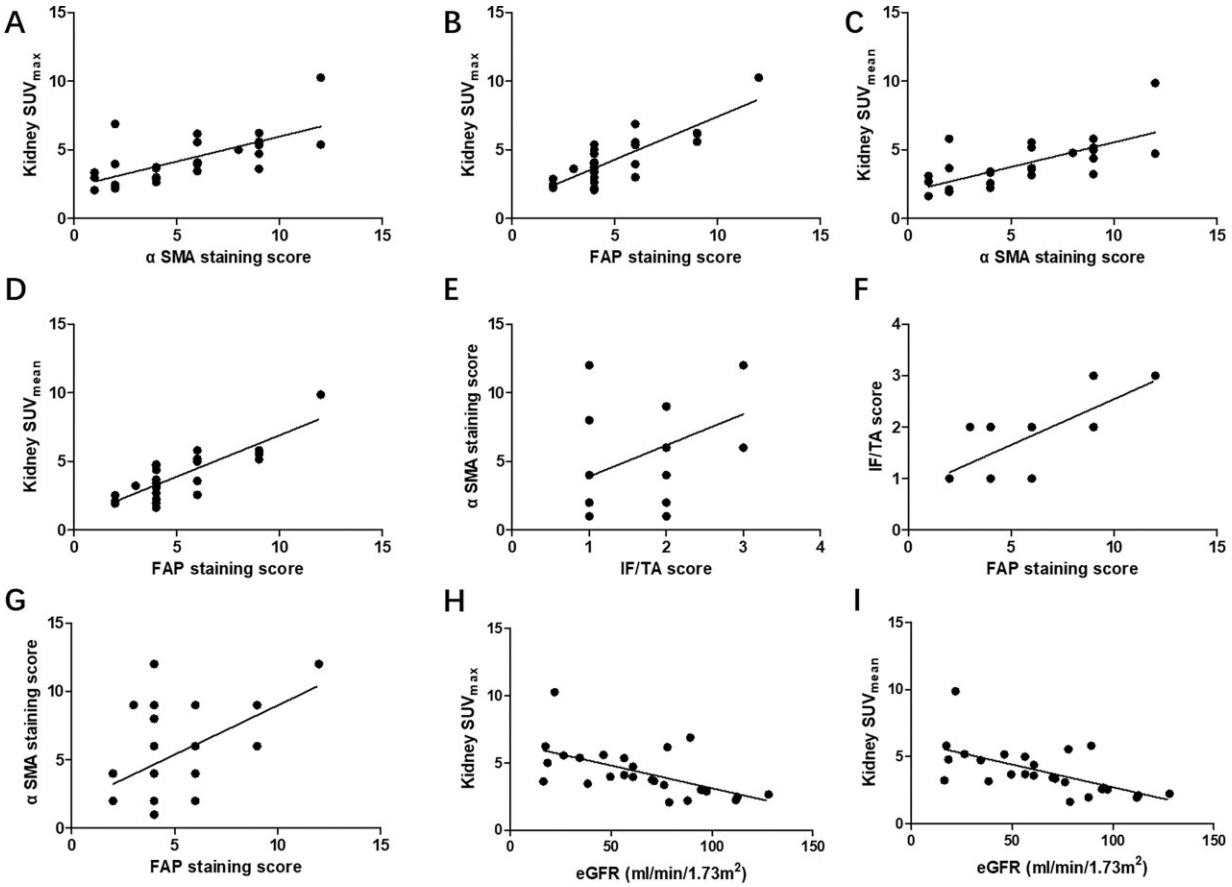

Figure 7: Correlation of the renal parenchymal FAPI uptake with immunohistochemical staining and eGFR levels. (**A**) The SUV_{max} showed a positive correlation with the staining score for αSMA ($r = 0.686$, $P < 0.001$). (**B**) The SUV_{max} exhibited a positive correlation with the staining score for FAP ($r = 0.732$, $P < 0.001$). (**C**) The SUV_{mean} showed a positive correlation with the staining score for αSMA ($r = 0.667$, $P < 0.001$). (**D**) The SUV_{mean} exhibited a positive correlation with the staining score for FAP ($r = 0.739$, $P < 0.001$). (**E**) The IF/TA score demonstrated a positive correlation with the staining score for αSMA ($r = 0.438$, $P < 0.05$). (**F**) The IF/TA score demonstrated a positive correlation with the staining score for FAP ($r = 0.590$, $P < 0.05$). (**G**) The staining score for αSMA demonstrated a positive correlation with the staining score for FAP ($r = 0.420$, $P < 0.05$). (H) The SUV_{max} exhibited a significant negative correlation with the eGFR levels ($r = -0.683$, $P < 0.001$). (I) The SUV_{mean} exhibited a significant negative correlation with the eGFR levels ($r = -0.614$, $P = 0.001$).

non-selective enrolment of patients with various kidney diseases, therefore considered a broader range of renal diseases. In this study, the intense FAPI uptake is observed in kidneys affected by acute interstitial nephritis characterized by high inflammation or mesangial proliferative nephropathy associated with significant fibrosis indicated both acute and chronic kidney diseases can exhibit increased FAPI uptake.

There are several limitations that should be acknowledged in this study. First, despite our efforts to investigate and compare FAPI uptake in kidney diseases with different renal pathologies, the limited number of enrolled patients may not suffice for a comprehensive analysis. Future studies would benefit from a larger cohort to ensure robust conclusions regarding the utility of FAPI-PET/CT in assessing renal inflammation and interstitial fibrosis. Second, due to the lack of PET/CT imaging follow-up after treatment, longitudinal comparisons were precluded. Third, it is necessary to develop improved methods and parameters for measuring renal parenchymal FAPI uptake to minimize the impact of residual radiotracer on the renal pelvis and calyces or other confounding factors.

CONCLUSIONS

The PET/CT imaging with [^{18}F] AlF-NOTA-FAPI-04 can provide a comprehensive and non-invasive assessment of tubular injury in diverse kidney diseases. Further investigations are warranted to support its value in clinical practice.

SUPPLEMENTARY DATA

Supplementary data are available at *ckj* online.

FUNDING

This work was supported by Science and Technology Project of Sichuan Provincial Health Commission (23LCYJ023), Basic research project of Science and Technology Department of Yunnan Province (202101AT070148), Natural Science Foundation of Sichuan Province (2023NSFSC0635), and Sichuan Province Science and Technology Support Programme (23SYSX0132).

DATA AVAILABILITY STATEMENT

The data used to support the findings of this study are available from the corresponding author upon request.

CONFLICT OF INTEREST STATEMENT

None declared.

REFERENCES

1. Black LM, Lever JM, Agarwal A. Renal inflammation and fibrosis: a double-edged sword. *J Histochem Cytochem* 2019;**67**:663–81. https://doi.org/10.1369/0022155419852932
2. Panizo S, Martínez-Arias L, Alonso-Montes C *et al*. Fibrosis in chronic kidney disease: pathogenesis and consequences. *Int J Mol Sci* 2021;**22**:408. https://doi.org/10.3390/ijms22010408
3. Meng XM. Inflammatory mediators and renal fibrosis. *Adv Exp Med Biol* 2019;**1165**:381–406. https://doi.org/10.1007/978-981-13-8871-2_18
4. Ferenbach DA, Bonventre JV. Mechanisms of maladaptive repair after AKI leading to accelerated kidney ageing and CKD. *Nat Rev Nephrol* 2015;**11**:264–76. https://doi.org/10.1038/nrneph.2015.3
5. Meran S, Steadman R. Fibroblasts and myofibroblasts in renal fibrosis. *Int J Exp Pathol* 2011;**92**:158–67. https://doi.org/10.1111/j.1365-2613.2011.00764.x
6. Klinkhammer BM, Lammers T, Mottaghy FM *et al*. Noninvasive molecular imaging of kidney diseases. *Nat Rev Nephrol* 2021;**17**:688–703. https://doi.org/10.1038/s41581-021-00440-4
7. Jiang K, Ferguson CM, Lerman LO. Noninvasive assessment of renal fibrosis by magnetic resonance imaging and ultrasound techniques. *Transl Res* 2019;**209**:105–20. https://doi.org/10.1016/j.trsl.2019.02.009
8. Rankin AJ, Mayne K, Allwood-Spiers S *et al*. Will advances in functional renal magnetic resonance imaging translate to the nephrology clinic. *Nephrology (Carlton)* 2022;**27**:223–30. https://doi.org/10.1111/nep.13985
9. Aertgeerts K, Levin I, Shi L *et al*. Structural and kinetic analysis of the substrate specificity of human fibroblast activation protein alpha. *J Biol Chem* 2005;**280**:19441–4. https://doi.org/10.1074/jbc.C500092200
10. Levy MT, McCaughan GW, Abbott CA *et al*. Fibroblast activation protein: a cell surface dipeptidyl peptidase and gelatinase expressed by stellate cells at the tissue remodelling interface in human cirrhosis. *Hepatology* 1999;**29**:1768–78. https://doi.org/10.1002/hep.510290631
11. Fitzgerald AA, Weiner LM. The role of fibroblast activation protein in health and malignancy. *Cancer Metastasis Rev* 2020;**39**:783–803. https://doi.org/10.1007/s10555-020-09909-3
12. Rosenkrans ZT, Massey CF, Bernau K *et al*. [(68) Ga]Ga-FAPI-46 PET for non-invasive detection of pulmonary fibrosis disease activity. *Eur J Nucl Med Mol Imaging* 2022;**49**:3705–16. https://doi.org/10.1007/s00259-022-05814-9
13. Li M, Younis MH, Zhang Y *et al*. Clinical summary of fibroblast activation protein inhibitor-based radiopharmaceuticals: cancer and beyond. *Eur J Nucl Med Mol Imaging* 2022;**49**:2844–68. https://doi.org/10.1007/s00259-022-05706-y
14. Dendl K, Koerber SA, Kratochwil C *et al*. FAP and FAPI-PET/CT in malignant and non-malignant diseases: a perfect symbiosis. *Cancers (Basel)* 2021;**13**:4946. https://doi.org/10.3390/cancers13194946
15. Kratochwil C, Flechsig P, Lindner T *et al*. (68)Ga-FAPI PET/CT: tracer uptake in 28 different kinds of cancer. *J Nucl Med* 2019;**60**:801–5. https://doi.org/10.2967/jnumed.119.227967
16. Mao H, Chen L, Wu W *et al*. Noninvasive assessment of renal fibrosis of chronic kidney disease in rats by [(68)Ga]Ga-FAPI-04 small animal PET/CT and biomarkers. *Mol Pharm* 2023;**20**:2714–25. https://doi.org/10.1021/acs.molpharmaceut.3c00163
17. Zhou Y, Yang X, Liu H *et al*. Value of [(68)Ga]Ga-FAPI-04 imaging in the diagnosis of renal fibrosis. *Eur J Nucl Med Mol Imaging* 2021;**48**:3493–501. https://doi.org/10.1007/s00259-021-05343-x
18. Conen P, Pennetta F, Dendl K *et al*. [(68) Ga]Ga-FAPI uptake correlates with the state of chronic kidney disease. *Eur J Nucl Med Mol Imaging* 2022;**49**:3365–72. https://doi.org/10.1007/s00259-021-05660-1
19. Lyu Z, Han W, Zhao H *et al*. A clinical study on relationship between visualization of cardiac fibroblast activation protein activity by Al(18)F-NOTA-FAPI-04 positron emission tomography and cardiovascular disease. *Front Cardiovasc Med* 2022;**9**:921724. https://doi.org/10.3389/fcvm.2022.921724
20. Jiang X, Wang X, Shen T *et al*. FAPI-04 PET/CT using [(18)F]AlF labeling strategy: automatic synthesis, quality control, and in vivo assessment in patient. *Front Oncol* 2021;**11**:649148. https://doi.org/10.3389/fonc.2021.649148
21. Braune A, Oehme L, Freudenberg R *et al*. Comparison of image quality and spatial resolution between (18)F, (68)Ga, and (64)Cu phantom measurements using a digital Biograph Vision PET/CT. *EJNMMI Phys* 2022;**9**:58. https://doi.org/10.1186/s40658-022-00487-7
22. Levey AS, Stevens LA, Schmid CH *et al*. A new equation to estimate glomerular filtration rate. *Ann Intern Med* 2009;**150**:604–12. https://doi.org/10.7326/0003-4819-150-9-200905050-00006
23. Gomes MF, Mardones C, Xipell M *et al*. The extent of tubulointerstitial inflammation is an independent predictor of renal survival in lupus nephritis. *J Nephrol* 2021;**34**:1897–905. https://doi.org/10.1007/s40620-021-01007-z
24. Wang S, Zhou X, Xu X *et al*. Clinical translational evaluation of Al(18)F-NOTA-FAPI for fibroblast activation protein-targeted tumour imaging. *Eur J Nucl Med Mol Imaging* 2021;**48**:4259–71. https://doi.org/10.1007/s00259-021-05470-5
25. Meng XM, Nikolic-Paterson DJ, Lan HY. Inflammatory processes in renal fibrosis. *Nat Rev Nephrol* 2014;**10**:493–503. https://doi.org/10.1038/nrneph.2014.114
26. Grande MT, Pérez-Barriocanal F, López-Novoa JM. Role of inflammation in túbulo-interstitial damage associated to obstructive nephropathy. *J Inflamm* 2010;**7**:19. https://doi.org/10.1186/1476-9255-7-19
27. Lee SB, Kalluri R. Mechanistic connection between inflammation and fibrosis. *Kidney Int Suppl* 2010;**78**:S22–6. https://doi.org/10.1038/ki.2010.418
28. Liu BC, Tang TT, Lv LL *et al*. Renal tubule injury: a driving force toward chronic kidney disease. *Kidney Int* 2018;**93**:568–79. https://doi.org/10.1016/j.kint.2017.09.033
29. Venkatachalam MA, Weinberg JM, Kriz W *et al*. Failed tubule recovery, AKI-CKD transition, and kidney disease progression. *J Am Soc Nephrol* 2015;**26**:1765–76. https://doi.org/10.1681/ASN.2015010006

Received: 13.12.2023; Editorial decision: 16.2.2024

© The Author(s) 2024. Published by Oxford University Press on behalf of the ERA. This is an Open Access article distributed under the terms of the Creative Commons Attribution-NonCommercial License (https://creativecommons.org/licenses/by-nc/4.0/), which permits non-commercial re-use, distribution, and reproduction in any medium, provided the original work is properly cited. For commercial re-use, please contact journals.permissions@oup.com